Surface and Coatings Technology, Volume 204, Issue 23, 25 August 2010, Pages 3851-3857

Accepted Manuscript

Evolution of stress and morphology in thermal barrier coatings

Xin Wang, Alan Atkinson, Laura Chirivì, John R. Nicholls

PII: S0257-8972(10)00332-4
DOI: doi: 10.1016/j.surfcoat.2010.04.065
Reference: SCT 15720

To appear in: *Surface & Coatings Technology*

Received date: 21 January 2010
Accepted date: 28 April 2010

Evolution of Stress and Morphology in Thermal Barrier Coatings

Xin. Wang[a] and Alan Atkinson[a], Laura Chirivì [b]and John R. Nicholls[b]

a Department of Materials, Imperial College London SW7 2BP, UK

b Cranfield University, Cranfield, Bedford MK43 0AL, UK

Abstract

Residual stress in the thermally grown oxide (TGO) in thermal barrier coatings (TBCs) was measured by photoluminescence piezospectroscopy (PLPS) and stress maps created to track local stress changes as a function of thermal cycling. The local stress images were observed to be correlated with morphological features on the metal surface that were purposely introduced during specimen preparation. Local stress relaxation and morphological evolution with thermal cycling were studied using the stress maps combined by post-mortem SEM examination. It was found that the morphology in the specimen having an initial polished surface was quite stable, while that in the specimen with a rough surface was unstable. The average residual stress in the specimen with the unstable morphology decreased with thermal cycling and it eventually failed along TGO/YSZ interface. The specimen with stable morphology maintained a high TGO stress throughout the thermal cycling process and failed along TGO/bond coat interface. The rough surface was also found to give rise to the formation of transition alumina (θ-Al_2O_3) in the TGO which was correlated with a reduced TGO stress.

Key words: TBCs; Stress Mapping; Luminescence Spectroscopy; Interface Morphology; Failure Mechanism

1 Introduction

Thermal barrier coatings (TBCs) are applied on turbine blades in both land-based power generation gas turbines and airplane engines to improve the performance and efficiency of the engines. Subjected to high temperature oxidation and cyclic heating and cooling service conditions, TBCs degrade in both thermal protection capability and mechanical stability, as a result of a combination of thickening of the alumina thermally grown oxide (TGO), sintering of the top layer (YSZ), and weakening of critical interfaces. Eventually TBC top coating falls off from the metallic substrate after a certain period of service. However, the actual failure mechanisms of TBCs often turn out to be much more complicated. Detailed mechanistic descriptions of TBC failure mechanisms can be found in the literature [1-5]

TBCs typically have two ceramic layers (YSZ and TGO) and two metallic components (bond coat and substrate). It is believed that the driving force for the TBC spallation is the stored energy in ceramic layers resulting from the thermal expansion mismatch between metallic materials and ceramic layers when the component is cooled [1, 6]. Therefore, the measurement of the residual stress in the TGO is important for achieving a better understanding of TBC failure. Photo-luminescence piezo-spectroscopy (PLPS) is an optical technique for stress determination in alumina and alumina-containing ceramics [7, 8]. Its high spatial resolution and fast acquisition make it a powerful non-destructive evaluation tool for characterisation of thermal barrier coatings. PLPS has been employed in several studies to characterise the stress in the TGO in TBC systems [9-12] and efforts have been made to relate the residual stress in TGO to the remaining lifetime of the TBCs [13, 14]. However, the thermal mismatch stress in TGO can be relaxed by a variety of mechanisms. Therefore the relationship between residual stress and remaining TBC lifetime cannot be established without gaining a better understanding of coating failure mechanisms and stress relaxation in TGO.

The mechanics associated with the TBC coating failure are not fully understood. TBCs have been observed to fail in quite different ways; sometimes within the YSZ coating, sometimes along the TGO/bond coat interface, and sometimes at the TGO/YSZ interface [2, 15]. Surface roughness has been found to have a large effect on TGO residual stress and TBC lifetime [16-18] and to influence the oxidation of the bond coat at high temperature [19]. The interface morphology in some TBC systems has been observed to be unstable in that so-called “rumpling” of the TGO occurs and its amplitude grows with the cyclic oxidation [20-22]. These interface morphological instabilities can lead to the formation of cracks which are the nuclei for coating failure. The interface morphology instabilities have been suggested to be due to thermal expansion mismatch, phase transformations, and bond coat swelling [5, 23], as well as being influenced by the mechanical properties of the bond coat [24]. The main purpose of the current work was to investigate the interrelation between interface morphology and TGO residual stress and the effect of morphological changes on coating failure. In this work, firstly specimens with known morphological features were studied by PLPS. The stress variations obtained from luminescence mapping were found to match the major morphological features introduced purposely during specimen preparation. Then two specimens prepared with different surface roughness were subjected to thermal cycling and characterised by luminescence mapping. It was found that grit-blasting of substrate surface led to stress distributions with irregular patterns, while surface polishing led to regular stress distributions. Changes in the stress distributions were related to the morphological changes as thermal cycling progressed. Due to the high spatial resolution capability of PLPS, the spatial

distribution of θ-Al_2O_3 and stress relaxation by local θ-Al_2O_3 presence was also examined in detail by luminescence mapping.

2 Experimental

Two different Thermal Barrier Coating (TBC) systems were prepared and studied in the present work:

a TBC system with a Pt-diffused bond coat, and

a TBC system with a Pt-modified aluminide bond coat.

The Pt-modified aluminide bond coat has the β-(Pt,Ni)Al microstructure (i.e. NiAl with Pt in solid solution), while the Pt-diffused bond coat retains the γ - γ' microstructure of the superalloy substrate. Hence the Pt-diffused bond coat has a much higher creep resistance than the Pt-modified aluminide bond coat at high temperature. These two different bond coats could therefore exhibit different stress build-up and relaxation characteristics during thermal cycling and consequently, different failure mechanisms of TBCs.

The substrates adopted for both systems consisted of small disks of CMSX-4, 15mm in diameter and 3mm in thickness.

The TBC systems with a Pt-diffused bond coat were manufactured at the National High Temperature Surface Engineering Centre of Cranfield University. One dimensional roughness was introduced by mechanically grinding the substrate (CMSX-4) surface in one direction, generating an array of grooves all parallel to each other. One of the specimens had coarse and deep grooves on its surface, whereas the other one had relatively fine and shallow grooves. The grinding procedure was carried out in an Edgetek 5 axis super abrasive machine by Holroyd. The ground coupons were then coated with a 10μm thick layer of Platinum by DC magnetron sputtering at a pressure of $7*10^{-3}$ mbar using a Nordiko2500 unit. The coupons were heat treated for 1 hour at 1190 ˚C in vacuum, in order to produce a bond coat with the γ - γ' structure. At this stage, the grooves machined onto the substrate were still evident on the surface of the bond coat and the surface roughness was assessed using a Talysurf profilometer, measured along a direction perpendicular to the main irregularities. The Ra parameter for the coarse ground specimen was 1.165μm while for the fine ground specimen was 0.682μm. The specimens were finally coated with a 200μm thick layer of YSZ by Electron Beam Physical Vapour Deposition (EBPVD).

The TBC system with a Pt aluminide (β structure) bond coats were provided by Chromalloy UK Ltd. The detailed manufacturing procedure for this set of specimens were given in [25]. Here only a brief summary is given. The superalloy substrate was first subjected to a grit-blast using alumina grit and then a layer of Pt was deposited by electroplating, followed by heat treatment at 1050-1100˚C and pack-aluminising process. The specimens had two different bond coat surface finishes. For the specimen having 'normal' surface finish the YSZ ceramic top was deposited directly onto the surface after producing the bond coat for which the roughness was measured as Ra=5 μm. For the specimen with 'polished' surface, the bond coat surface was polished with 1 μm diamond paste and had an Ra of 0.5 μm. The YSZ top

coat was applied by EBPVD at 1000˚C in an argon/oxygen background atmosphere. The YSZ top coat thickness for the specimens with normal surface was ~70 μm and for the specimens with polished surface was ~100 μm.

Thermal cycling was conducted using a rig in which the specimen was moved in and out of a furnace by a computer-controlled motion stage. The temperature of the furnace was maintained at either 1135˚C or 1150˚C. Immediately after being removed from the furnace the specimens were fan-cooled by laboratory air. The specimens dwelt at high temperature for 1 h and stayed out of the furnace for 30 minutes. The specimens were removed at specified intervals for the luminescence measurements.

For TGO residual stress measurement, luminescence spectra were acquired using a Renishaw Raman optical microprobe (model 2000) fitted with a motorised mapping stage. The laser source was a green Ar^+ laser with a wavelength of 514.5 nm. An air conditioning unit was used to maintain a stable room temperature at 22±0.3°C. Before and after each experiment, the spectrometer was calibrated by taking a spectrum from a strain-free single crystal sapphire sample.

An acquisition time of one second was used for each spectrum collection. For high spatial resolution mapping, an objective lens, 50X (075NA) was used, which is capable of delivering a spot size of 1-2 μm. The mapping area was 300 × 200 μm and the pitch size was 5 μm. For even higher resolution mapping, an objective lens, 100X (095NA) was used, which is capable of delivering a spot size of < 1 μm. The mapping area was varied for different purposes and the pitch size was 1 or 2 μm.

In order to track back to the same area on the specimen after different thermal treatments, reference points that not only survive high temperature treatments, but also have geometrical stability all the time are critical for mapping accurately the stress evolution. For this purpose three micro-indentation marks aligned in a straight line were made on each specimen surface. The Vickers indents were about 70 microns in diagonal length. The sharp corners of the indents were found to be quite stable during the heat treatment and be ideal reference points. Position registering between successive maps with an error less than 5μm was achieved.

In addition, stress relaxation near a specimen edge has been observed in a separate study of TBC systems (unpublished). Such relaxation only occurred under the YSZ within a short distance (~10 μm) of the edge. In this study, care was taken to choose a mapping area which was well away from the edges (typically >0.2mm) to exclude the effect of edge creep relaxation on stress evolution.

Since the R2 luminescence line of α-alumina has a nearly linear dependence on stress [8, 10], all the peak shift data in this paper are of the R2 line. For the convenience of presentation, the peak shift in this paper is expressed as a positive number. In reality the peak shift is negative due to a compressive residual stress in TGO.

3 Results

3.1 Residual stress in TGO on Pt diffusion bond coats with known morphology

The specimens with Pt diffusion bond coats were examined using PLPS after 20 thermal cycles at 1150˚C. Fig.1 shows peak shift (stress) maps for both specimens. A peak shift of 5 cm^{-1} corresponds approximately to a biaxial stress of 1 GPa. In both cases the shift is large and corresponds to a residual stress of 5-6 GPa. The specimen which had the coarse ground substrate (Fig.1a) clearly exhibits one dimensional features in the TGO stress distribution, whereas the fine ground specimen (Fig.1b) does not show any similar features. The stress variations in Fig.1b are quite randomly-positioned.

Both specimens failed after about 37 thermal cycles and post-mortem SEM examination was conducted on spalled pieces of coating and exposed substrate surfaces. It was found that both specimens failed along the TGO/bond coat interface. The under side of the coating pieces spalled from the coarse ground specimen was covered predominantly by Al_2O_3 (Fig.2a) and longitudinal features are clearly visible. The under side of the coating spalled from the fine ground specimen was also covered in Al_2O_3. However, the longitudinal features could not be seen until the electron beam was incident on the specimen surface at a shallow angle. As shown in Fig.2b, the one dimensional features were then visible, but they are much shallower than for the coarse ground specimen.

3.2 Residual stress in the TGO on Pt-Al bond coats with different surface conditions.

These specimens were subjected to thermal cycling at 1135°C and luminescence mapping was carried out periodically. Sequential mapping was conducted on the same areas of each specimen in order to follow how the local features develop.

Figs.3a-c show how the stress distribution in one particular area of the specimen with normal surface finish evolved from 63^{rd} cycle to 103^{rd} cycle. The average stress in the TGO for this sample (approximately 1 GPa) was much lower than that for the ones with Pt diffusion bond coats and decreased gradually with thermal cycling. However, some larger changes occurred locally. For example the stress around the area ‘A’ in Fig. 3 decreased significantly with thermal cycling; the low stress region ‘B’ in Fig.3b disappeared after further cycling in Fig.3c; and a new low stress zone ‘C’ has appeared in Fig.3c.

In contrast, no major changes in stress distribution were observed for the specimen with the polished surface (Figs. 4a-c) and the mean stress was much higher (approximately 3.5 GPa). The maps show well-defined regions that have stresses higher and lower than the average and these regions remain in the same place as thermal cycling proceeds.

Fig. 5 gives the TGO stress evolution as a function of thermal cycling for the two specimens with Pt-Al bond coats. The TGO stress in the specimen with normal surface finish was initially very low (~5 cm^{-1}, or 1GPa), quickly increased to 2 GPa within a few cycles, and then decreased gradually with further thermal cycling. In contrast, the TGO stress in the specimen with the polished surface was much higher (~4 GPa) and remained at this high level (Fig.4b).

The approximate θ- Al_2O_3 content in the TGO was estimated using the following equation [26]:

$$C_\theta = \frac{A_{14330} + A_{14546} + A_{14626}}{A_{14330} + A_{14546} + A_{14626} + A_{R1} + A_{R2}} \quad \text{Eq. 1}$$

where A_{14330}, A_{14546} and A_{14626} are the areas of luminescence peaks centred at 14330 cm^{-1}, 14546 cm^{-1} and 14626 cm^{-1} respectively and A_{R1} and A_{R2} are the peak areas of the characteristic R1 and R2 peaks. The evolution θ- Al_2O_3 content with thermal cycling is also given in Figs.5a and b for the specimens with Pt-Al bond coats. The θ- Al_2O_3 content in the specimen with normal surface finish was much higher than that in the polished one. The θ- Al_2O_3 content in both specimens decreased with thermal cycling, but the θ- Al_2O_3 content in specimen with normal surface finish experienced a dramatic decrease in the first 25 cycles and after that the θ- Al_2O_3 content change was much slower.

Luminescence mapping with a pitch size of 2 μm was conducted to reveal detailed local stress variation. Many very low stress region (as arrowed in Fig.6a) were seen in the normal surface finish specimen, which were only a few microns in size. In contrast, the residual stress in the polished specimen was quite uniform even at high resolution, as shown in Fig.6b.

Thermal cycling was terminated at the 105th cycle for the normal surface specimen and at 75th cycle for the polished specimen and the coatings were intact at this stage. However, the coatings on both specimens were found to have failed after leaving for two months at room temperature and in ambient atmosphere. SEM was used to investigate the failure mode. It was found the failure locus for the specimen with normal surface finish was along the TGO/YSZ interface while that for the polished specimen was along the TGO/bond coat interface. Figs.7a and b give the SEM images of the exposed substrates. The TGO layer stayed on the normal surface finish substrate with sporadic YSZ residual grains. Conversely the polished specimen (Fig.7b) has only small amount of residual TGO left on bond coat.

X-ray diffraction was used to examine the phase composition of the failed TBC. No monoclinic phase zirconia was seen in the ceramic, so the room temperature failure was not due to tetragonal to monoclinic transformation. The failure was probably caused by moisture-assisted subcritical spall propagation [27]. However, further detailed investigation is needed to substantiate this speculation.

4 Discussion

4.1 Stress redistribution by interface roughness

Figs.1a and 2a clearly shows that bond coat surface roughness influences TGO residual stress. These two figures have a similar magnification and hence it is evident that the number of linear features in the stress map (Fig.1a) is fewer than in the SEM image (Fig.2a). In earlier studies [11] we showed that the luminescence mapping has a resolution of <5 μm and so luminescence mapping should have been able to pick up features corresponding to all the parallel grooves in Fig.2a if they were all capable of influencing TGO stress to a similar extent. Furthermore, the luminescence mapping of the specimen with the fine ground surface

shows no indication of linear features. These observations indicate that the amplitude of surface roughness has to be larger than a critical value to have a significant influence on the TGO stress distribution. Since the roughness for the coarse ground specimen was Ra=1.165μm and that for the fine ground specimen was Ra=0.682μm, so the critical roughness should be between 0.682 and 1.165.

The effect of local curvature on the peak shift of the luminescence from TGO has been assessed using a composite cylinder model in a previous paper [26] and by Gong and Clarke for a sinusoidal TGO (but without top coat)[28]. According to the models, the peak shift of a concave curvature should be almost the same as that for a flat surface, while the peak shift at a convex location is smaller by an amount depending on the curvature (as reflected in the amplitude and wavelength of the TGO roughness compared with the TGO thickness). Therefore, in Fig.1a the strips with relatively large peak shift correspond to local concave curvature (valleys), while the strips with relatively small peak shift correspond to local convex curvature (peaks).

4.2 The effect of surface roughness on morphological evolution and failure

Since stress mapping is sensitive to the morphological features, stress maps could be used to track morphological changes during thermal cycling. However, it must be borne in mind that other factors influence local TGO stress, such as damage, and therefore variations in stress do not necessarily relate directly to surface morphology. Nevertheless, one interpretation of the low stress areas in Figs.3 and 4 is that they corresponding to local peaks in the bond coat surface and the high stress areas correspond to local valleys. The irregular shapes of the high and low stress areas in Figs.3a-c are consistent with the irregular surface morphology resulting from the grit blasting during specimen preparation. Similarly, the more regular stress variation seen for the polished specimen in Figs. 4a-c is consistent with a gradual rumpling of the bond coat/TGO interface resulting from thermal exposure.

The rough interface introduced in the manufacturing of the specimen with normal surface finish favours further short wavelength roughening of the interface which facilitates the formation of local cracks between top coat and TGO [24]. Eventually this leads to weakening of the YSZ/TGO interface and finally delamination at this interface driven by the release of stored elastic energy within the YSZ.

Conversely the specimen with the polished surface maintained a relatively flat bond coat/TGO interface throughout the thermal cycling process with only relatively gentle, long wavelength morphology and hence no large local relaxation of the TGO stress. Thus the TGO/YSZ interface was not degraded in this case and eventual failure was by delamination along the bond coat/TGO interface driven by the release of stored elastic energy within both the TGO and the YSZ.

4.3 The effect of the θ- Al_2O_3 content on the TGO residual stress

From Figs.5a and b it is clear that the TGO in the specimen with normal surface finish Pt-Al bond coat had a much higher θ-Al_2O_3 content than that with the polished bond coat, especially in the early stage. This suggests that the polished surface favours the formation of

the stable α- Al_2O_3, while the rough surface encourages the formation of the transition phase θ- Al_2O_3. Also from Fig.5a, the TGO stress increases as the θ- Al_2O_3 content decreases.

The correlation between θ- Al_2O_3 content and TGO residual stress was investigated further using the data from the 2501 spectra acquired for the luminescence map of the specimen with normal surface finish after 25 cycles. The transition phase content as a function of peak shift is plotted in Fig.8. It can be seen that the peak shift tends to increase as the transition phase content decreases. The reduction in the stress in the α-Al_2O_3 could be due to the θ-Al_2O_3 having a lower elastic modulus and/or a higher CTE than α-Al_2O_3. High resolution luminescence mapping (area 30 x 20 μm and pitch size 1 μm) was conducted within a small area to reveal the distributions of the θ-Al_2O_3 and TGO stress. As shown in Fig.9a the θ-Al_2O_3 was not uniformly distributed, but was preferentially located in the lower region of the mapped area. Fig.9b is the corresponding peak shift map and shows that the higher stress region matches the region with lower θ-Al_2O_3 content quite well. The low stress areas associated with the transition phase are only a few microns in extent (Fig.9b) and similar in size to the small regions of low stress seen as "speckles" in Figs. 3a-c. These can be attributed to the existence of the θ- Al_2O_3. From Figs. 3a-c, it is clear the number of the "speckles" decreases with thermal cycling, which is consistent with the θ- Al_2O_3 content decreasing with thermal cycling as shown in Fig.5a.

When significant transition θ-alumina was present in the TGO, the regions within the θ-Al_2O_3 that subsequently transformed to α- Al_2O_3 are placed under a tensile strain due to the volume decrease associated with the phase transformation. Thus the presence of transition θ alumina is an extra contributor to the stress evolution apart from the morphology.

It is far from being fully understood as to why and how transition θ- alumina is formed. In a separate study [26], we found that, despite two turbine blades having been subjected to identical thermal treatments, and supposed to have the same chemical composition and manufacturing procedure, they had significantly different θ content at convex parts of the blades. The result from the present study and that from [26] both seem to indicate that the kinetics of the formation of the θ- Al_2O_3 and its transformation to α- Al_2O_3 could be changed significantly by subtle changes in chemical composition, interface morphology or defect content in the TBC system. Further investigation is needed.

5 Summary and Conclusions

In this paper, it was observed that TGO stress distributions obtained by luminescence mapping of specimens with different degrees of one dimensional surface roughness can reflect morphological features of the bond coat/TGO interface because sharp curvature in the TGO can give rise to significant local stress relaxation. The interface roughness is also reflected in the frequency distribution, which is narrower for the smoother interface.

Thus the TGO stress maps for a coating on a substrate with a normal grit-blasted surface and Pt-Al bond coat showed irregular patterns and low average stress due, at least in part, to relaxation by local TGO bending. Conversely, a similar specimen with a polished surface

had much higher mean TGO stress and the maps showed more regular longer wavelength variations, possibly caused by slight interface rumpling.

The luminescence maps show that the TGO stress distribution for the specimen with the normal surface finish is not stable with thermal cycling (i.e. some low stress regions appear to move) and there was a gradual lowering of TGO stress with thermal cycling. This is interpreted as the result of changing interface morphology due to rumpling. It leads to local separation of the TGO/YSZ/ interface, which is thereby weakened, and finally this interface delaminates driven by the release of stored elastic energy within the YSZ. Conversely the polished specimen had a high TGO residual stress comparable with the theoretical thermal mismatch stress throughout thermal cycling and the interface morphology was stable. This specimen eventually delaminated along the bond coat/TGO interface driven by the release of stored elastic energy within both the TGO and the YSZ.

The TGO stress is also influenced by the presence of transition alumina (θ-Al_2O_3) in the TGO, in addition to TGO morphology, and high transition alumina content was correlated with low TGO stress.

Acknowledgement:

The authors thank EPSRC for financial support (grant GR/T07329/01), Prof. L. Cohen for access to the Raman microprobe and Dr. Karen Yates and Dr. Robert Maher for help in setting up the instrument. The authors also thank Dr David Rickerby of Rolls Royce plc and Mr Rodney Wing of Chromalloy UK for provision of the specimens with Pt-Al bond coats.

References

[1] A. G. Evans, D. R. Mumm, J. W. Hutchinson, G. H. Meier and F. S. Pettit, Prog. Mater. Sci 46 (2001) 505.

[2] D. R. Mumm and A. G. Evans, Acta. Mater. 48 (2000) 1815.

[3] N. P. Padture, M. Gell and E. H. Jordan, Science 296 (2002) 280.

[4] V. K. Tolpygo and D. R. Clarke, Acta. Mater. 48 (2000) 3283.

[5] D. S. Balint and J. W. Hutchinson, J. Mech. Phys. Solids.53 (2005) 949.

[6] D. M. Lipkin, D. R. Clarke, M. Hollatz, M. Bobeth and W. Pompe, Corros. Sci. 39 (1997) 231.

[7] Q. Ma and D. R. Clarke, J. Am. Ceram. Soc. 77 (1994) 298.

[8] J. He and D. R. Clarke, J. Am. Ceram.Soc.78 (1995) 1347.

[9] A. Selcuk and A. Atkinson, Mat Sci Eng A-Struct. 335 (2002) 147.

[10] A. Selcuk and A. Atkinson, Acta. Mater. 51 (2003) 535.

[11] X. Wang and A. Atkinson, Mat Sci Eng A-Struct 465 (2007) 49.

[12] M. Gell, S. Sridharan, M. Wen and E. H. Jordan, Int. J. Appl. Ceram. Technol. 1 (2004) 316.

[13] M. Wen, E. H. Jordan and M. Gell, J Eng Gas Turb Power 128 (2006) 610.

[14] S. Sridharan, L. D. Xie, E. H. Jordan and M. Gell, Surf. Coat. Tech.179 (2004) 286.

[15] R. A. Handoko, J. L. Beuth, G. H. Meier, F. S. Pettit and M. J. Stiger, in "Durable Surfaces" (2001) p. 165.

[16] D. B. Zhang, S. K. Gong, H. B. Xu and Z. Y. Wu, Surf. Coat. Tech. 201 (2006) 649.

[17] J. Liu, J. W. Byeon and Y. H. Sohn, Surf. Coat. Tech. 200 (2006) 5869.

[18] L. D. Xie, Y. H. Sohn, E. H. Jordan and M. Gell, Surf. Coat. Tech.176 (2003) 57.

[19] A. Gil, V. Shemet, R. Vassen, M. Subanovic, J. Toscano, D. Naumenko, L. Singheiser and W. J. Quadakkers, Surf. Coat. Tech. 201 (2006) 3824.

[20] W. A. Mei, H. J. B. Eric and M. Gell, Surf. Coat. Tech. 201 (2006) 3289.

[21] V. K. Tolpygo and D. R. Clarke, Script. Mater. 57 (2007) 563.

[22] V. K. Tolpygo, D. R. Clarke and K. S. Murphy, Surf. Coat. Tech. 188-89 (2004) 62.

[23] A. W. Davis and A. G. Evans, Metall. Mater. Trans. A 37A (2006) 2085.

[24] J. Shi, S. Darzens and A. M. Karlsson, Mat Sci Eng A-Struct 392 (2005) 301.

[25] G. Lee, Surf. Coat. Tech.201 (2006) 3931.

[26] X. Wang, G. Lee and A. Atkinson, Acta. Mater. 57 (2009) 182.

[27] V. Sergo and D. R. Clarke, J. Am. Ceram. Soc. 81 (1998) 3237.

[28] X. Gong, Oxid Met. 50 (1998) 355.

Figure captions

Fig. 1 Peak shift (stress) maps for TGO in coatings with Pt diffusion bond coat on a) one-dimensionally coarse ground; and b) one dimensionally fine ground substrates after 25 cycles at 1150°C. Mapping area is 300 µm by 200 µm and pitch size 5 µm.

Fig.2 Scanning electron micrograph of the reverse side of the TBC coatings spalled from a) one-dimensionally coarse ground; and b) one dimensionally fine ground substrates with Pt diffusion bond coats. Al_2O_3 appears mid-gray.

Fig.3 Sequential peak shift (stress) maps of the same area on the specimen with Pt-Al bond coat and normal surface finish after a) 63^{rd} cycle, b) 83^{rd} cycle, c) 103rd cycle. The mapped area is 300 µm by 200µm and pitch size is 5 µm.

Fig.4 Sequential peak shift (stress) maps of the same area on the specimen with Pt-Al bond coat and polished surface finish after a) 25th cycle, b) 45th cycle, c)7 5th cycle. The mapped area is 300 µm by 200µm and pitch size is 5 µm

Fig.5 Evolution of average residual stress and θ-Al_2O_3 content with thermal cycling for specimens with Pt-Al bond coats and a) normal and b) polished surface finishes.

Fig.6 High resolution (50 µm by 50µm) peak shift (stress) maps after 25 cycles for specimens with Pt-Al bond coats and a) normal and b) polished surface finishes.

Fig.7 SEM images of the exposed substrate after failure for specimens with Pt-Al bond coats and different surface finishes: a) normal surface finish (white area is YSZ and gray area Al_2O_3); and b) polished surface finish (gray is bond coat and dark islands are residual TGO).

Fig.8 The correlation between peak shift and transition alumina content in the spectra acquired during mapping the TGO on the specimen with Pt-Al bond coat and normal surface finish after 25 cycles.

Fig.9 High resolution maps for the specimen with Pt-Al bond coat and normal surface finish after 25 cycles showing a) θ- Al_2O_3 content and b) peak shift (same area).

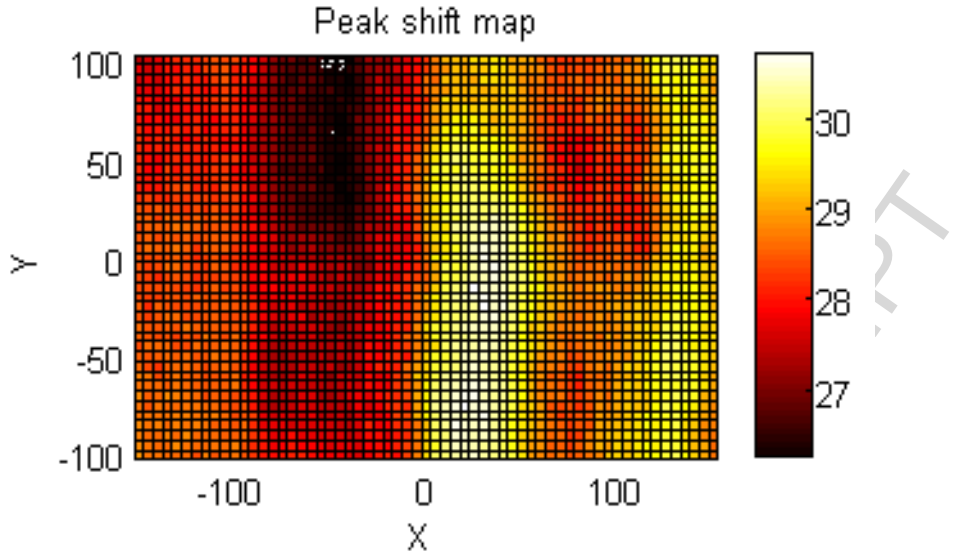

Fig.1a

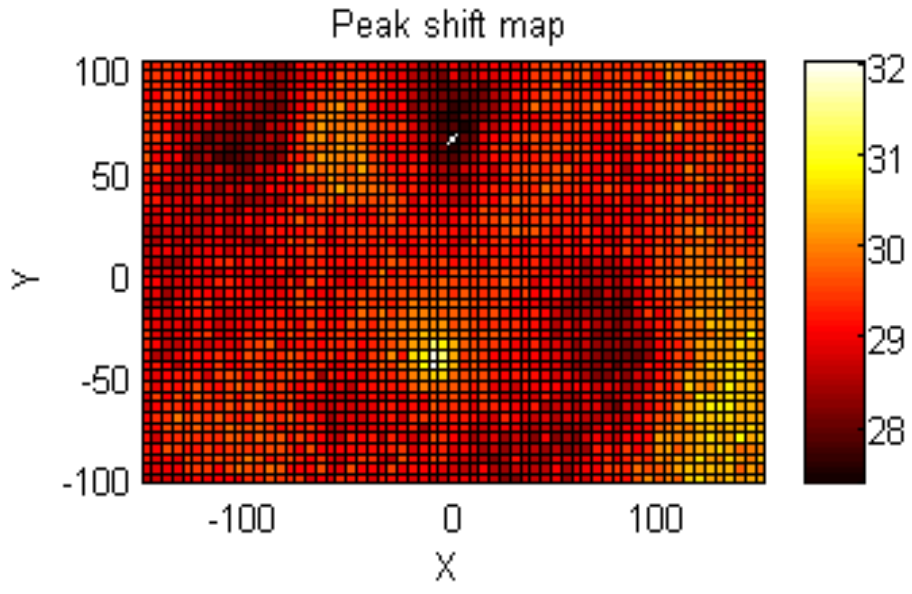

Fig.1b

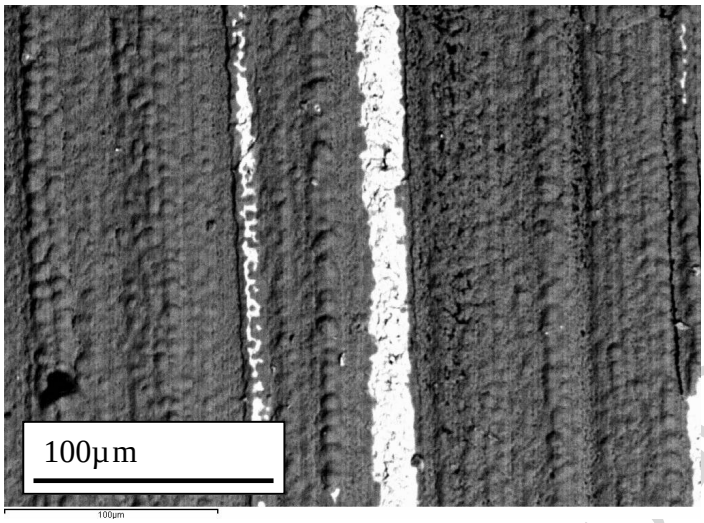

Fig.2a

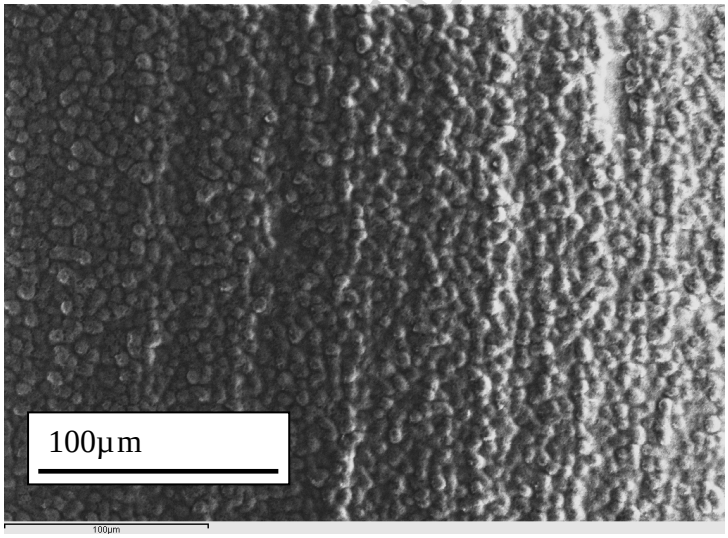

Fig.2b

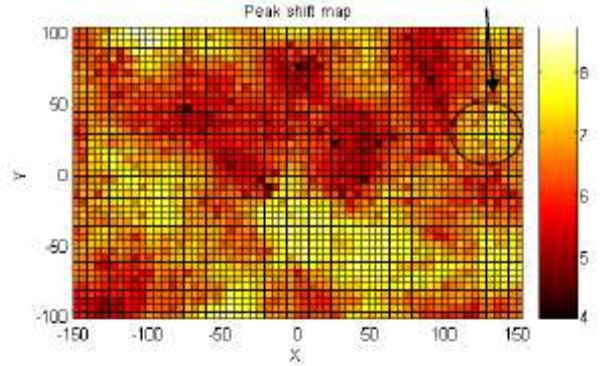

Fig.3a

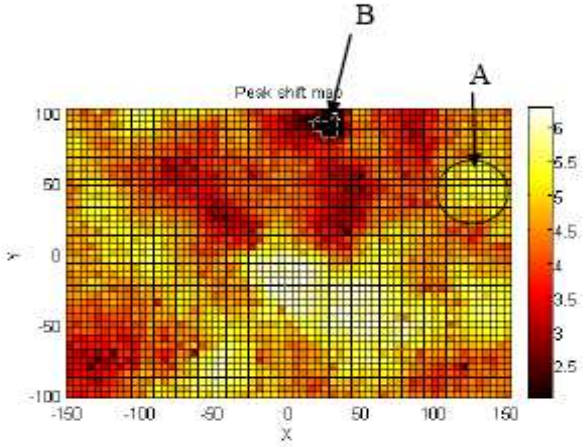

Fig.3b

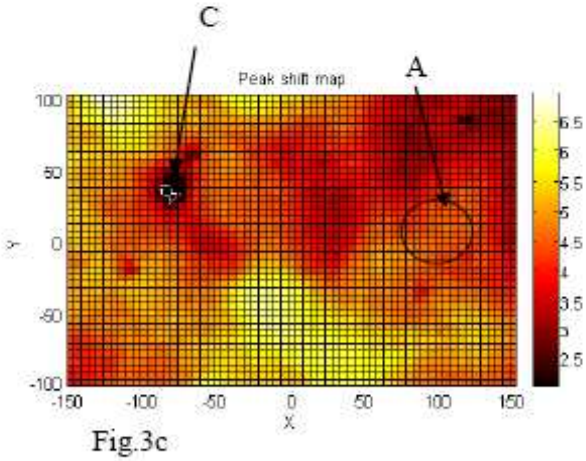

Fig.3c

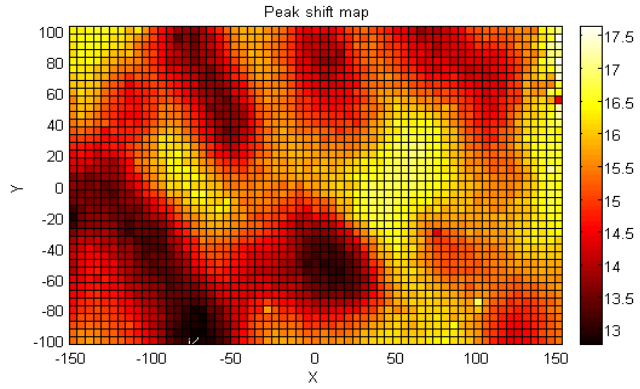

Fig.4a

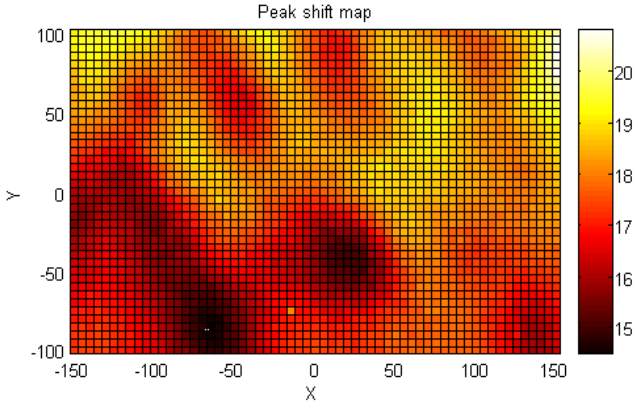

Fig.4b

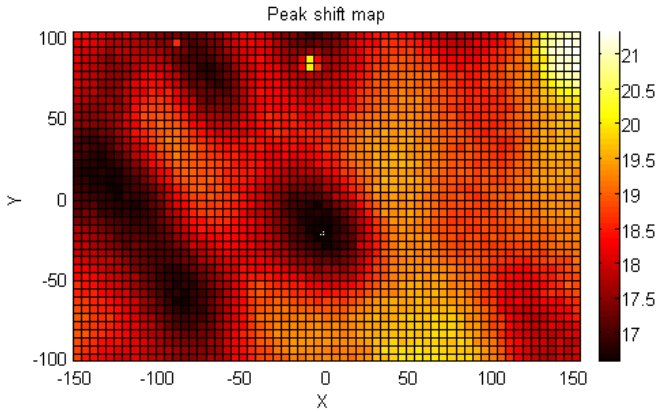

Fig.4c

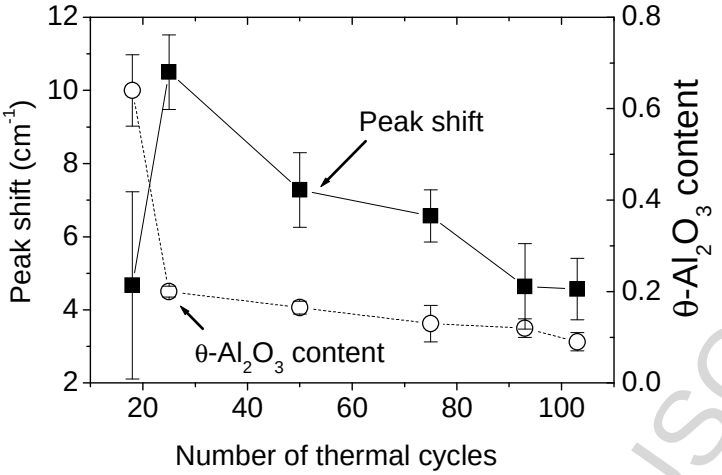

Fig.5a

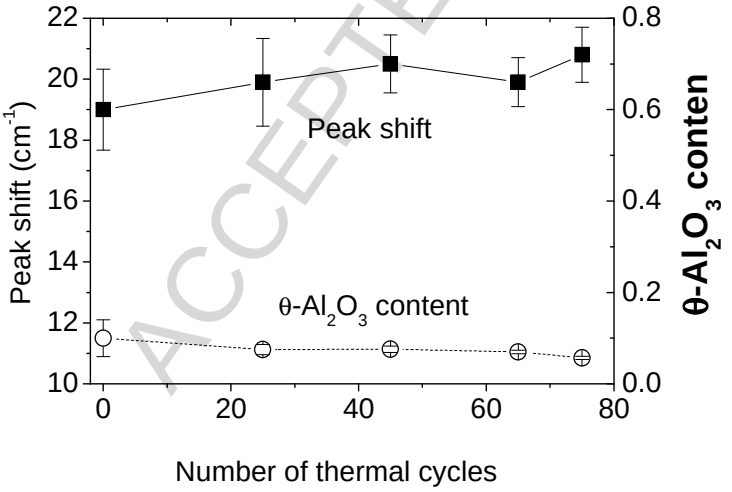

Fig.5b

Fig.6a

Fig.6b

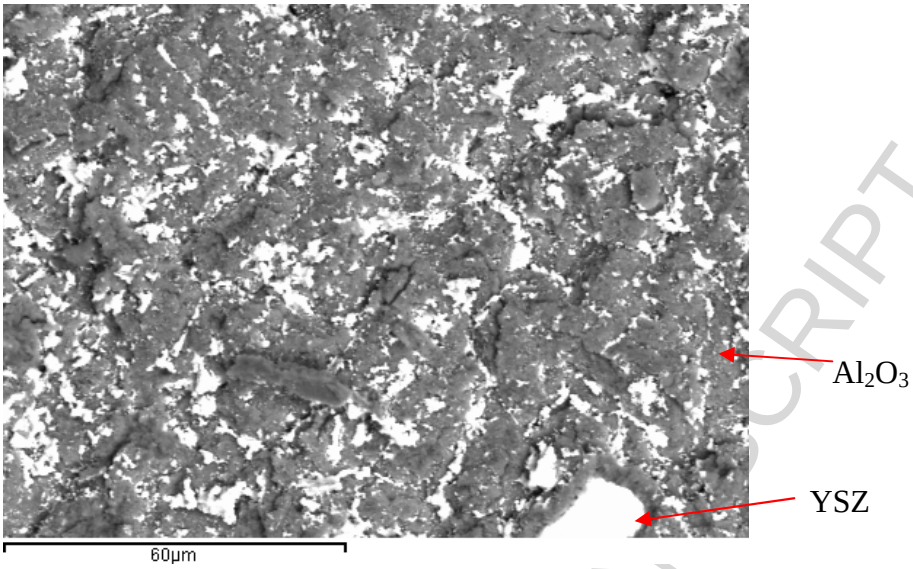

Fig.7a

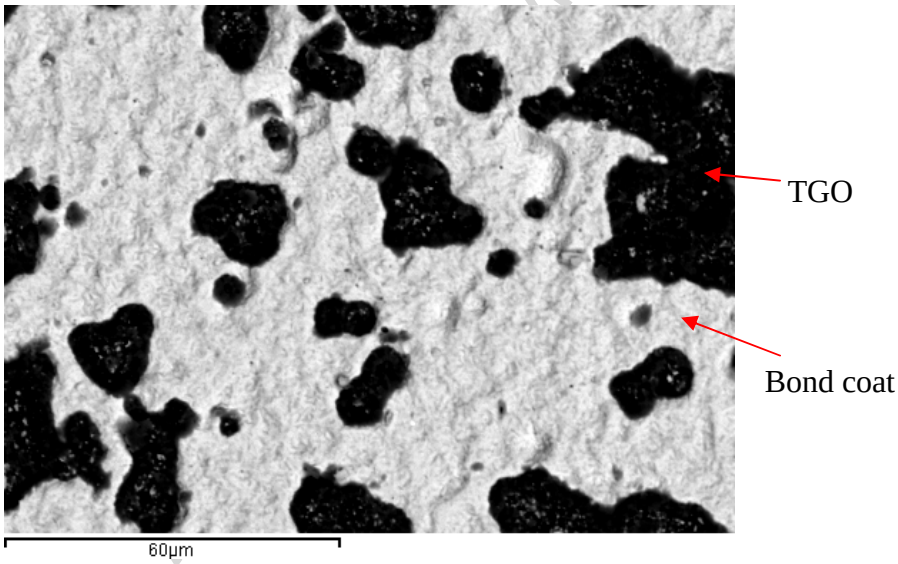

Fig.7b

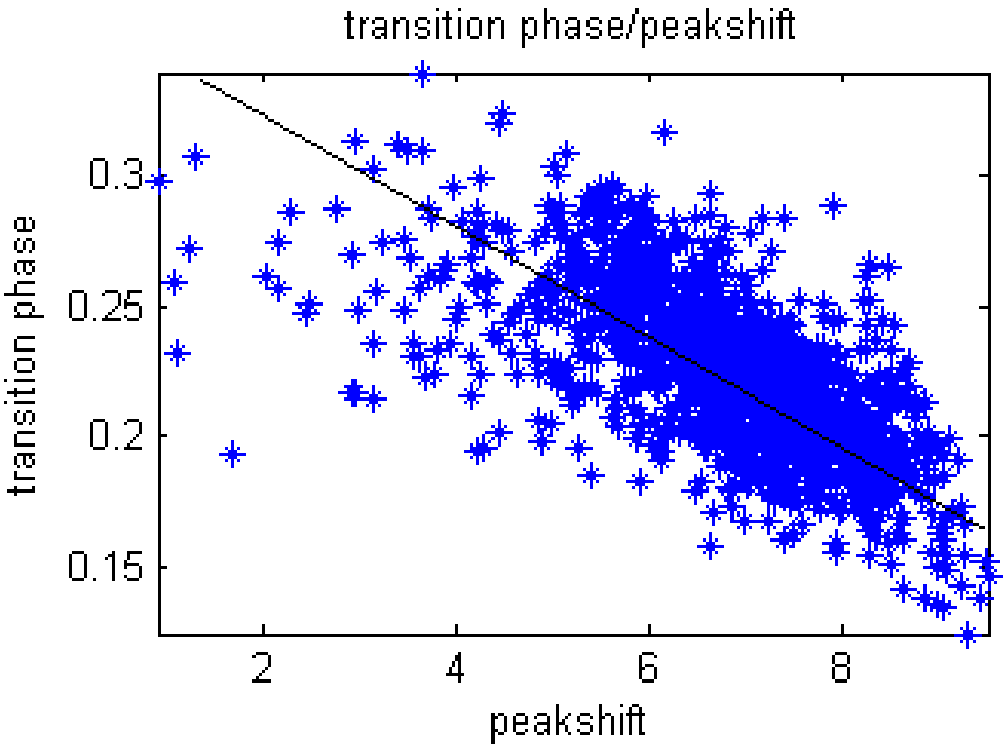

Fig.8

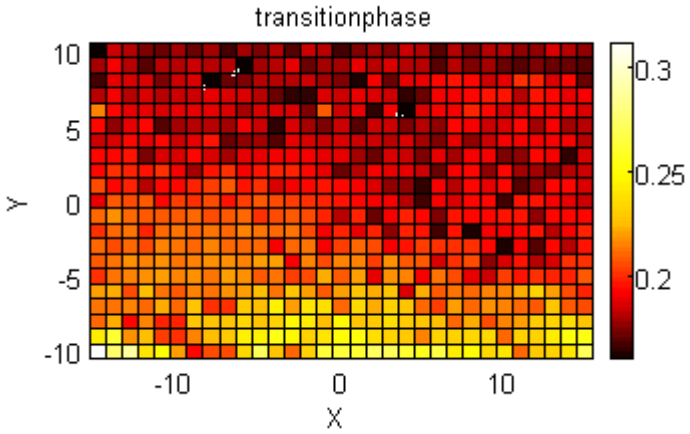

Fig.9a

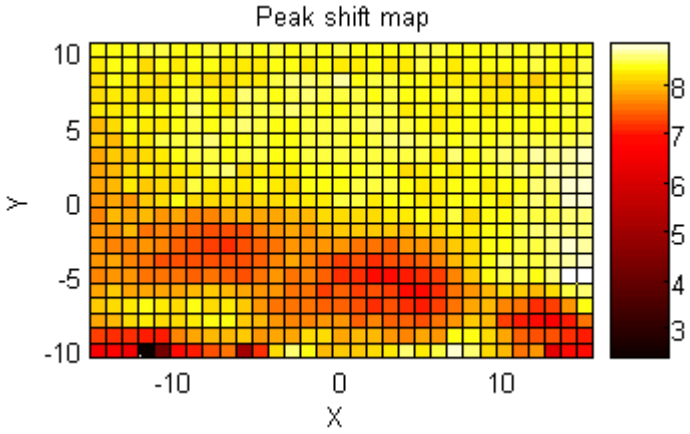

Fig.9b